



Article

Relationship between Lightning and Aerosol Optical Depth over the Uttarakhand Region in India: Thermodynamic Perspective

Alok Sagar Gautam ¹, Abhishek Joshi ², Sagarika Chandra ³, Umesh Chandra Dumka ^{4,*} , Devendraa Siingh ³ and Ram Pal Singh ⁵

¹ Department of Physics, Hemvati Nandan Bahuguna Garhwal University, Birla Campus, Srinagar 246174, India

² Department of Physics, Hemvati Nandan Bahuguna Garhwal University, SRT Campus, Badshahihaul, Srinagar 249199, India

³ Indian Institute of Tropical Meteorology, Dr. Homi Bhabha Road, Pashan, Pune 411088, India

⁴ Aryabhata Research Institute of Observational Sciences, Nainital 263001, India

⁵ Department of Physics, Banaras Hindu University, Varanasi 211005, India

* Correspondence: dumka@aries.res.in



Citation: Gautam, A.S.; Joshi, A.; Chandra, S.; Dumka, U.C.; Siingh, D.; Singh, R.P. Relationship between Lightning and Aerosol Optical Depth over the Uttarakhand Region in India: Thermodynamic Perspective. *Urban Sci.* **2022**, *6*, 70. <https://doi.org/10.3390/urbansci6040070>

Academic Editor:
Luis Hernández-Callejo

Received: 23 August 2022

Accepted: 3 October 2022

Published: 9 October 2022

Publisher's Note: MDPI stays neutral with regard to jurisdictional claims in published maps and institutional affiliations.



Copyright: © 2022 by the authors. Licensee MDPI, Basel, Switzerland. This article is an open access article distributed under the terms and conditions of the Creative Commons Attribution (CC BY) license (<https://creativecommons.org/licenses/by/4.0/>).

Abstract: The current study is mainly focused on the monthly variation in the lightning flash rate (LFR) and related thermodynamic parameters using the data for the years 2000–2013, and the trend of lightning variation is explored. Lightning data are used from a lightning imaging sensor (LIS) and an optical transient detector (OTP) boarded on the tropical rainfall measuring mission (TRMM). Additionally, aerosol optical depth (AOD) data at 550 nm for the same period were considered from a Moderate Resolution Imaging Spectroradiometer (MODIS). The assessment of lightning and AOD using monthly data makes it difficult to study seasonal contributions, and higher-resolution (hourly) data may be more appropriate, but unfortunately, no data were available with a higher resolution than monthly. The dependency of LFR is also investigated using thermodynamic/dynamic parameters. The LFR shows a moderate correlation with a correlation coefficient of 0.56, 0.62, and 0.63 for AOD, CAPE, and vertical velocity, respectively. The increasing AOD in the pre-monsoon season is associated with higher lightning flash rates over this region. The possible sources of aerosols that cause an increase in lightning activities are identified from the classification of aerosols based on the characteristic values of the AOD and the Ångström exponent. The thermodynamic relation of the Product of Bowen ratio with the sum of the precipitation rate and evaporation rate has been used as a proxy to evaluate the lightning flash rate density over Srinagar, Uttarakhand region (78.55° E–79.05° E, 29.97° N–30.47° N), with nine models from the Coupled Model Inter-comparison Project-Phase 5 (CMIP5). The model-simulated LFR has also been used for the projection of lightning in the late 21st century, and the projected LFR over the study area shows a 7.41% increase during the (2079–2088) period as compared to the historic period (1996–2005). The results of the study region indicate caution in using any single climate variable as a proxy for projecting a change in the lightning–climate relationships in the scenario of global warming.

Keywords: lightning; CAPE; AOD; NDVI; LFR; CMIP5

1. Introduction

Lightning is a naturally occurring phenomenon that originated in the high voltage differences in thunderstorms and exhibits currents as large as hundreds of kiloamperes. It is influenced by various atmospheric phenomena, as well as surface processes. Lightning causes damage to commercial installations, electrical and electronic equipment in homes and industrial facilities, and life [1–3]. Lightning and its intensity are governed by the form of moist convection, which is controlled by dynamics/thermodynamics, including

the roles of aerosols [1–9]. Several studies were conducted to understand the impact of aerosols on lightning [10–15]. The reduced droplet size in the presence of a high aerosol concentration [16–19] suppresses the collision and coalescence processes of droplets into raindrops, which eventually inhibits the warm rain process [20]. Atmospheric aerosols play an important role in the regulation and integration of deep convective clouds [16,21,22], which leads to higher lightning flashes in the moist environment [18,19,23,24]. Previous studies suggested that weak updraft generally corresponds to rainfall; on the other hand, deep and strong updraft leads to thunderstorm/lightning [24]. Increased aerosol concentrations (swelling effects) are reported in the presence of clouds with more than 99% humidity [25–28]. The observed positive correlation between effective cloud droplet radius and aerosols is explained to be caused by the humidity effect [29].

Aerosol loading, along with local meteorological parameters, affects the thermodynamic properties of the atmosphere and hence convective available potential energy (CAPE), which directly controls updraft strength and hence lightning intensity [30,31]. CAPE determines atmospheric instability in moist convection [32,33] and can be used as a proxy to lightning [34]. Many previous studies reported a positive correlation between lightning flash rate and CAPE [25–28,35–40]. Penki and Kamara [28] reported up to 22% of the change in lightning flash rate to be associated with CAPE. The role of orographic lifting was also observed in the increase in CAPE over the northeast region of the Himalayan foothills. A positive correlation ($R \sim 0.66, 0.69$) was found between the surface temperature with lightning over the Bay of Bengal and the Arabian sea [24]. A recent study reveals the positive relation between CAPE and surface temperature [41].

CAPE, moisture content, and local aerosol loading are also affected by vegetation cover and the health of vegetation, which is usually expressed in terms of the Normalized Difference Vegetation Index (NDVI). It plays an important role in global climate as well as it may also trigger mesoscale circulation. Vegetation cover interacts with the overlying atmosphere by changing the hydrological budget and surface energy. Deep-rooted forest areas can hold a significant amount of water which influences the latent heat flux, associated convective growth, and lightning activities. The role of NDVI in the distribution of lightning over the dry (northwest) and moist (northeast) regions of the Himalayas is noted [31]. A noticeable difference was found in the lightning flash density with a different type of vegetation cover in northern Australia [42]. Higher convective clouds over the deciduous forest in the hilly regions were reported in contrast to that in flat regions, while more convective cloud cover was observed over the farmlands located in the flat area.

Urban aerosol is also a big concern to mankind in terms of increased lightning activities. In this present study, we have analyzed the impact of aerosol loading on lightning over the western Himalayan region, which may be interesting to the scientific community as parts of the Himalayan region are among the hot spot of the World from a lightning flash rate point of view. In a recent study, Lal et al. [37] reported the impact of aerosol on lightning activity over the Indo-Gangetic Plain (IGP), a nearby region, but the western Himalayan region is still unexplored from this point of view [37]. So, in this study, we attempted to study the role of aerosol in lightning activities over this region.

In the present work, we mainly focused only on the monthly climatology of LFR concerning the other thermodynamic parameters to understand the pattern and trend of lightning. Apart from the aerosol, NDVI, CAPE, and other thermodynamic parameters, precipitation, evaporation, and surface heat fluxes (sensible heat flux and latent heat flux) play a major role in the formation of lightning flashes over any place. In a recent study [42], estimated that the NDVI plays a very important role in the transportation of heat in the form of latent heat flux from the vegetation, which may further act as a triggering mechanism for the formation of lightning activity in the northeast and northwest part of the Himalayan region. In some parts of the Himalayan region, it becomes difficult to pinpoint the suitable mechanism for the explanation of the connectivity/lightning. Therefore, some parameters or empirical relations may be required to determine the proper cause and estimation of lightning over the Himalayas. Recently [38], defined a proxy relation using this parameter

for the projected lightning flash rate over the Southeast Asian region. It was observed that, in some places, the effect of aerosol and vegetation index is very negligible, and the seasonal variation may be very less, but surface heat fluxes, precipitation, and evaporation were observed to play a very important role in the convective activity and lightning formation. Chandra et al. [38] used a thermodynamic relation $[BR (Pr + Er)]$, where BR is the Bowen ratio, Pr is the precipitation rate, and Er is the evaporation rate. They also used this relation as a proxy for the Lightning Flash Rate Density (LFRD) over the Southeast Asian region. In the present study, the same thermodynamic relation is used. Moreover, we are attempting to project the LFRD over the study region with this proxy relation using nine models from the Coupled Model Inter-comparison Project-Phase 5 (CMIP5). The present study may provide a direction for the use of the weekly/hourly or daily data in the near future for the forecast/prediction of LFR over this region; hence, it may be helpful for mitigation of lightning activity.

2. Area of Study

Figure 1 shows the lightning flash rate density distribution over the Indian subcontinent in which the study region is marked. There are two hotspots in the northeast and northwest regions of the northern Indian subcontinent. The moist convection over these regions is a result of the unique topography of both regions [43] (see Figure 2). A higher flash rate was observed over the NE region during the pre-monsoon season and over the NW region during the monsoon season [34]. Several lightning hotspots and deep convective storms were reported over these two regions [44]. It was observed in previous studies that the higher altitude regions (25° – 39° N) of the Indian subcontinent receive higher lightning events as compared to the low elevation region [45]. The northern region of the Indian subcontinent shows an arc of elevated lightning rate, which also includes the Himalayan foothills [26].

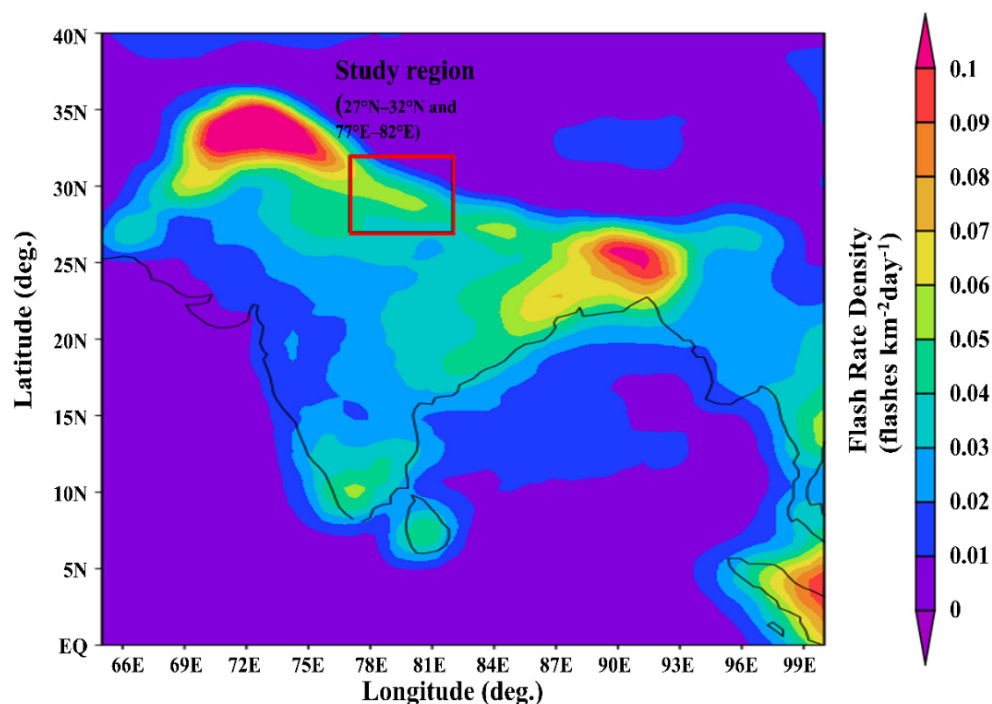


Figure 1. Mean lightning flash rate density for the period of 2000–2013 from combined lightning imaging sensor (LIS) and optical transient detector (OTD) observations.

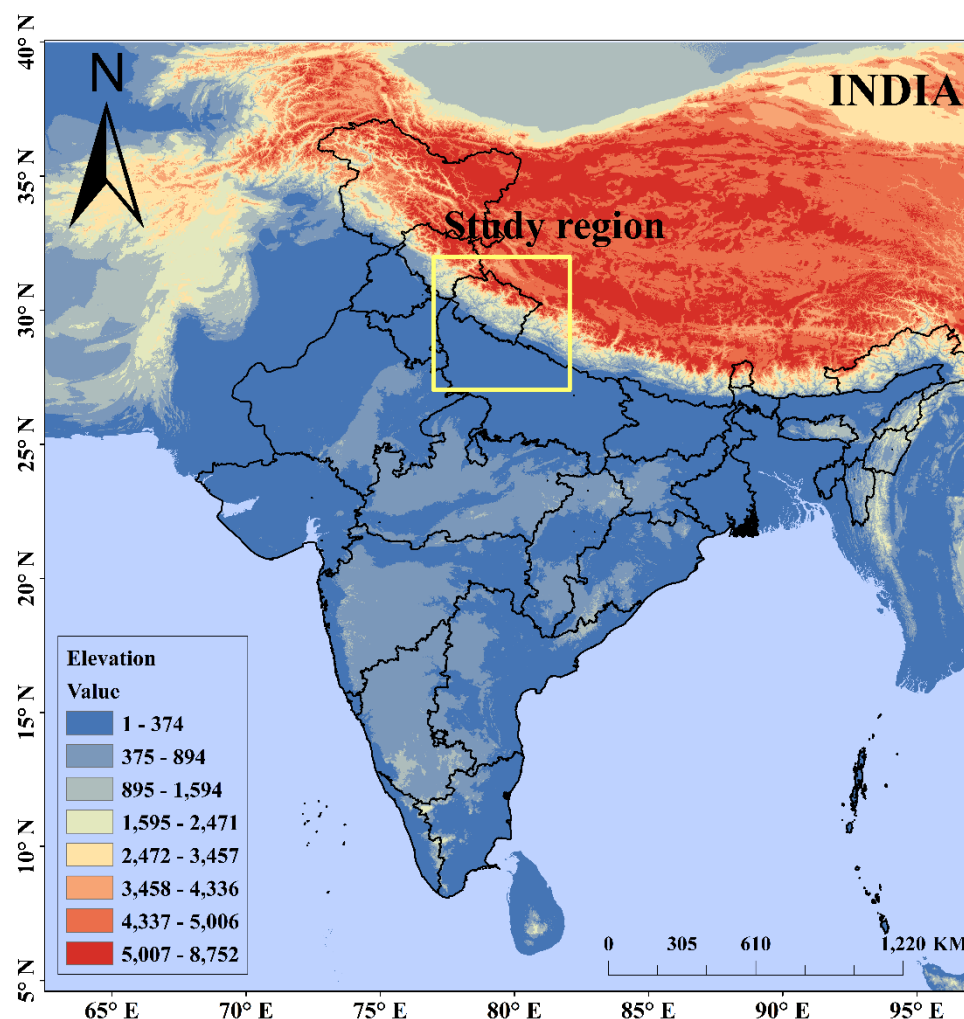


Figure 2. A topography map of the study region over the Indian subcontinent. The data were obtained from United State Geographical Survey (USGS) earth explorer digital elevation models (DEM) data.

The present study is focused on the central Himalayan foothill region between 27° – 32° N and 77° – 82° E ($5^{\circ} \times 5^{\circ}$), which includes Uttarakhand and western Uttar Pradesh (which is a part of the central IGP) of India. This region contains the highly elevated mountain tops and the plains of the Indo-Gangetic Basin, including the diversity of topography, vegetation cover, population density, and emission sources from industry. In this region, the central Himalayan high hills also support the orographic lifting of moist air, which results in higher convective activities over this region during the monsoon season. The IGP region of the Indian subcontinent contains heavy loading of aerosol originating from natural, as well as anthropogenic, activities. Urbanization and industrialization are the two main sources of higher aerosol production in this region, in addition to the transported aerosols from nearby western countries. For the projection of LFR over the study region, we only choose a small portion of the region with ($0.5^{\circ} \times 0.5^{\circ}$) box of Srinagar, Uttarakhand (78.55° E– 79.05° E, 29.97° N– 30.47° N).

3. Data and Methodology

The lightning flash rate was obtained from the space-borne observation of the lightning imaging sensor (LIS) and optical transient detector (OTD) onboard the tropical rainfall measurement mission satellite for 14 years (2000–2013) [46]. This dataset contains the total composite of bulk lightning production of both Intra-cloud (IC) and cloud-to-ground (CG) lightning with a nearly uniform detection efficiency of $73 \pm 11\%$ during daytime and

$93 \pm 4\%$ during nighttime. LIS has an observation time of 90 s for a point on the Earth's surface which is significant/sufficient to estimate the lightning flash rate over the region. High-resolution monthly climatology (HRMC) and low-resolution monthly time series (LRMTS) datasets were used in the present study with $0.5^\circ \times 0.5^\circ$ and $2.5^\circ \times 2.5^\circ$ spatial resolution, respectively.

Monthly averaged dataset of the aerosol optical depth (550 nm) and Ångström exponent (α) (412–470 nm) over the study region for the same period is obtained from the MODIS-TERRA Collection 6.1 [47]. Moderate Resolution Imaging Spectroradiometer (MODIS) is an instrument aboard terra (EOS AM-1) satellite and timed such that it passes the equator in the morning time covering the entire earth's surface in 1 to 2 days. The datasets are measured at $1^\circ \times 1^\circ$ resolution. The NDVI dataset (MOD13C2 v006) is also obtained from the MODIS-Terra platform with a spatial resolution of $0.05^\circ \times 0.05^\circ$. It may be noted that seasonal contribution of lightning and AOD could be better resolved if higher resolution (hourly) data were used in the analysis than monthly data but unfortunately no such data are available.

Monthly averaged meteorological parameters, including temperature, relative humidity, vertical velocity, total precipitation, CAPE, mean rates of precipitation, evaporation, surface sensible heat flux, and latent heat flux, were obtained from the ERA5 platform by ECMWF (European Centre for Medium-Range Weather Forecasts) reanalysis dataset [48]. Total precipitation data were later converted into the precipitation rate. The horizontal resolution of the datasets was $0.25^\circ \times 0.25^\circ$ for obtained reanalysis datasets. All datasets were averaged spatially to study the monthly and seasonal variations. To estimate proxy [(defined as the ratio of sensible heat flux to latent heat flux) and BR (Pr + Er)], with a grid resolution of $0.5^\circ \times 0.5^\circ$ were derived from the improved version of the European Centre for Medium-Range Weather Forecasts (ECMWF), ERA5 reanalysis products (<https://cds.climate.copernicus.eu>, accessed on 1 March 2022). For the projection of LFR, the Simulated precipitation rate (Pr), air temperature (T), and evaporation rate (Er) are obtained from the Coupled Model Inter-comparison Project Phase 5 (CMIP5, <http://cmip-pcmdi.llnl.gov/cmip5/>, accessed on 1 March 2022) data archive. In this work, a total of nine models are evaluated (CANESM2, CNRM-CM5, FGOALS-G2, GFDL-CM3, GFDL-ESM2M, GFDL-ESM2G, MIROC5, MIROC5-ESM-CHEM, and MIROC5-ESM). Models are selected as per the availability of all required parameters. These models were previously used and yielded better results [49–52]. In this study, the years 1996–2005 of the CMIP5 “historical” experiment represent the current climate, while the years 2079–2088 of the “RCP8.5” experiment represent the late 21st-century climate. For the simulation of LFR with different models, we use the relation, $LFR = K \times BR (Pr + Er)$, where LFR is the density of lightning flash rate in flashes $\text{km}^{-2} \text{day}^{-1}$, Pr is the precipitation rate in $\text{kg m}^{-2} \text{day}^{-1}$, and Er is the evaporation rate in $\text{kg m}^{-2} \text{day}^{-1}$. The precipitation rate has been taken in $\text{kg m}^{-2} \text{day}^{-1}$ instead of mm day^{-1} , and 1 mm of precipitation has been used in 1 kg m^{-2} of liquid water. The magnitude of BR describes the energy gained or lost from the earth's surface to the atmosphere. K is the proportionality constant with units as several flashes per kilogram of water. A detailed description of the proxy and the value of K is given in [45].

4. Results and Discussion

4.1. Spatial Distribution of Lightning

The spatial distribution of lightning flash rate density (LFRD) along with AOD, NDVI, and CAPE for seasonal climatology throughout the observation period are shown in Figures 3–6. The maximum number of lightning occurred during the pre-monsoon season (Figure 4), with the highest flash rate density over the central part of the study region (between 29° – 30° N and 79° – 80° E). During the same season, more aerosol loading is observed over the lower part of the study region (containing the western part of Uttar Pradesh, India). However, the vegetation index and CAPE are significantly low during the pre-monsoon season (Figure 4). This may be due to high temperature and less vapor

pressure. In contrast, in the monsoon season (Figure 5), the focus of the lightning density and the aerosol concentration shift toward the NW direction. In this season, the vegetation cover (>0.6) and CAPE values ($>800 \text{ J kg}^{-1}$) are observed to be the highest over the Himalayan foothills. The increased vegetation cover and deep-rooted forest area may have released latent heat [53]. A similar variation of vegetation cover was also reported [54]. Broader leaf plants release a large amount of water vapor into the atmosphere, which supports deep convection and increased CAPE [55].

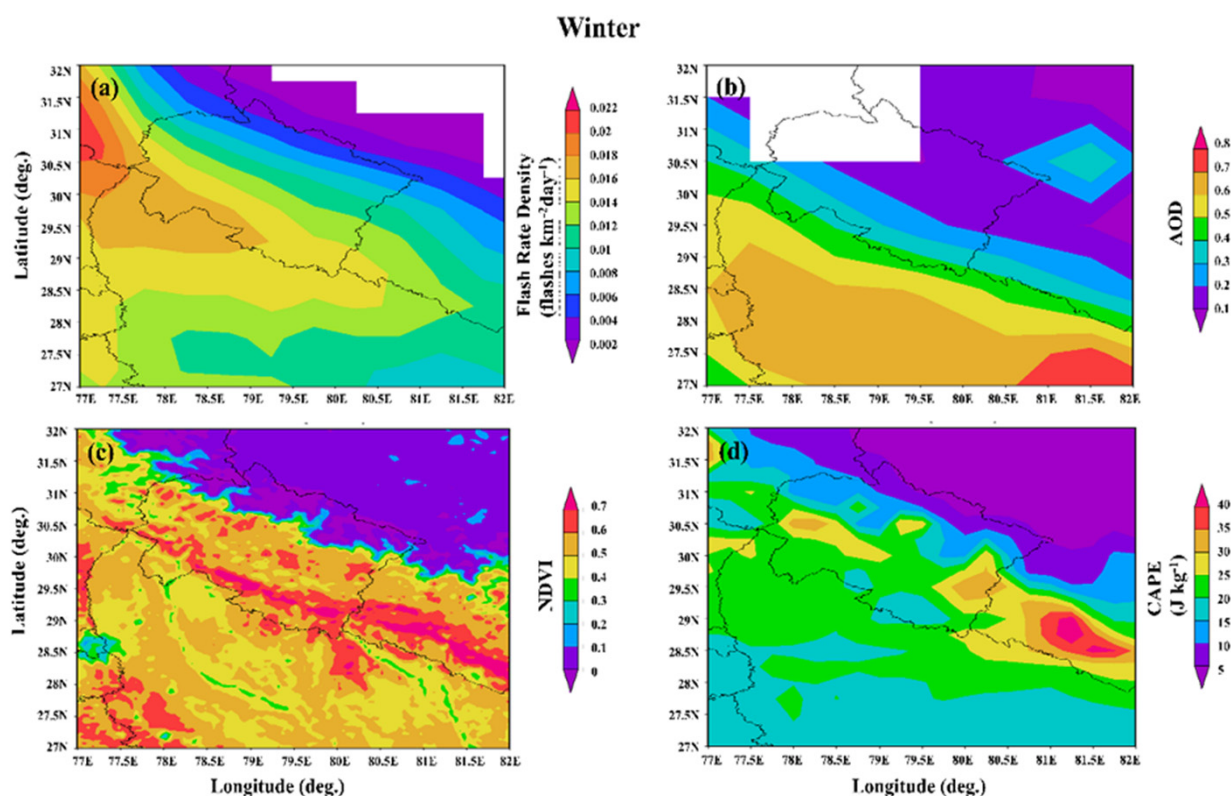


Figure 3. Spatial distribution of (a) LFRD, (b) AOD, (c) NDVI, and (d) CAPE for the winter season over the study region.

It is clear from the spatial distribution that the CAPE and vegetation index have the least contribution to the lightning activity over the central Himalayan region. However, the highest CAPE values were observed during the monsoon season (Figure 5), but the same is not reflected in the lightning activity. Increased aerosol loading is also observed over this region in winter (Figure 3) and post-monsoon season (Figure 6). Earlier studies suggested that the strong subsidence of aerosols leads to aerosol trapping generated by agricultural waste burning, and local industrial emission elevates the AOD values over the IGP region during the post-monsoon and winter season [56–58]. It is not reflected in lightning activity due to low convective activities as it was observed in the pre-monsoon season.

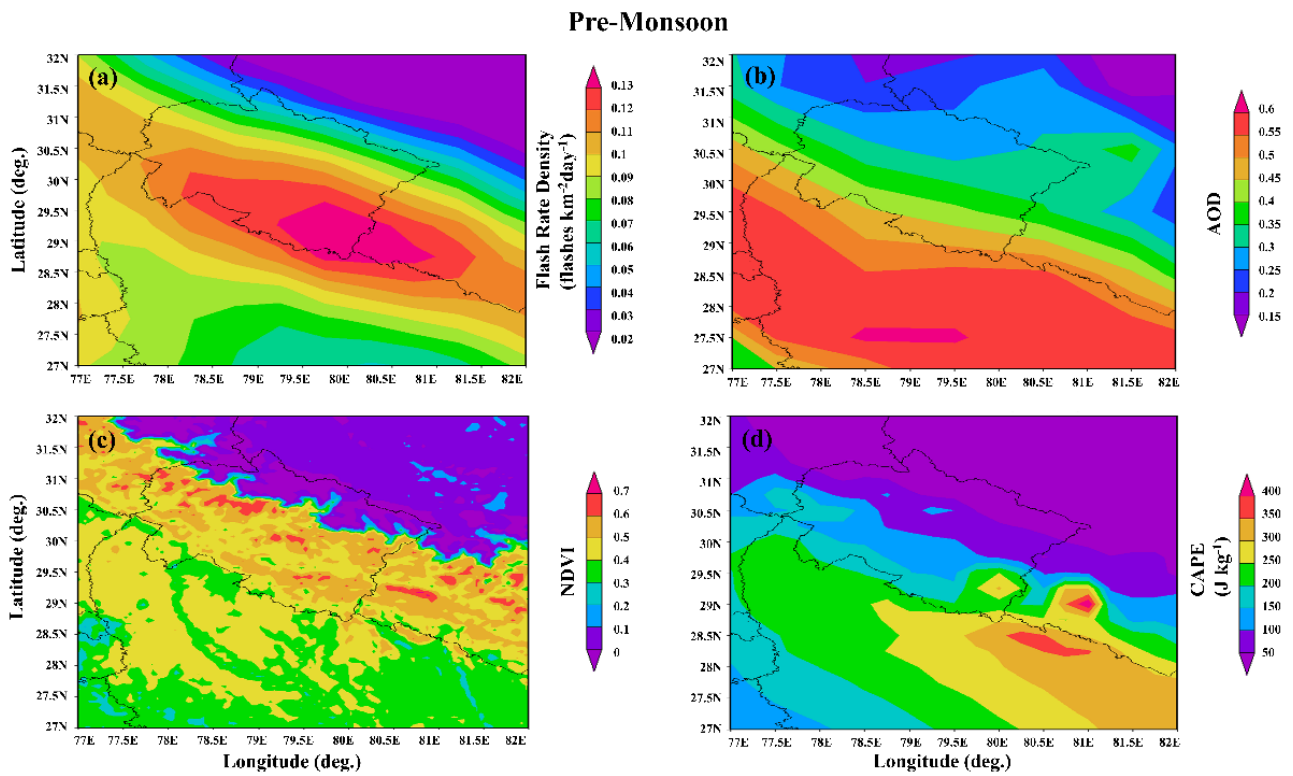


Figure 4. Spatial distribution of (a) LFRD, (b) AOD, (c) NDVI, and (d) CAPE for pre-monsoon season over the study region.

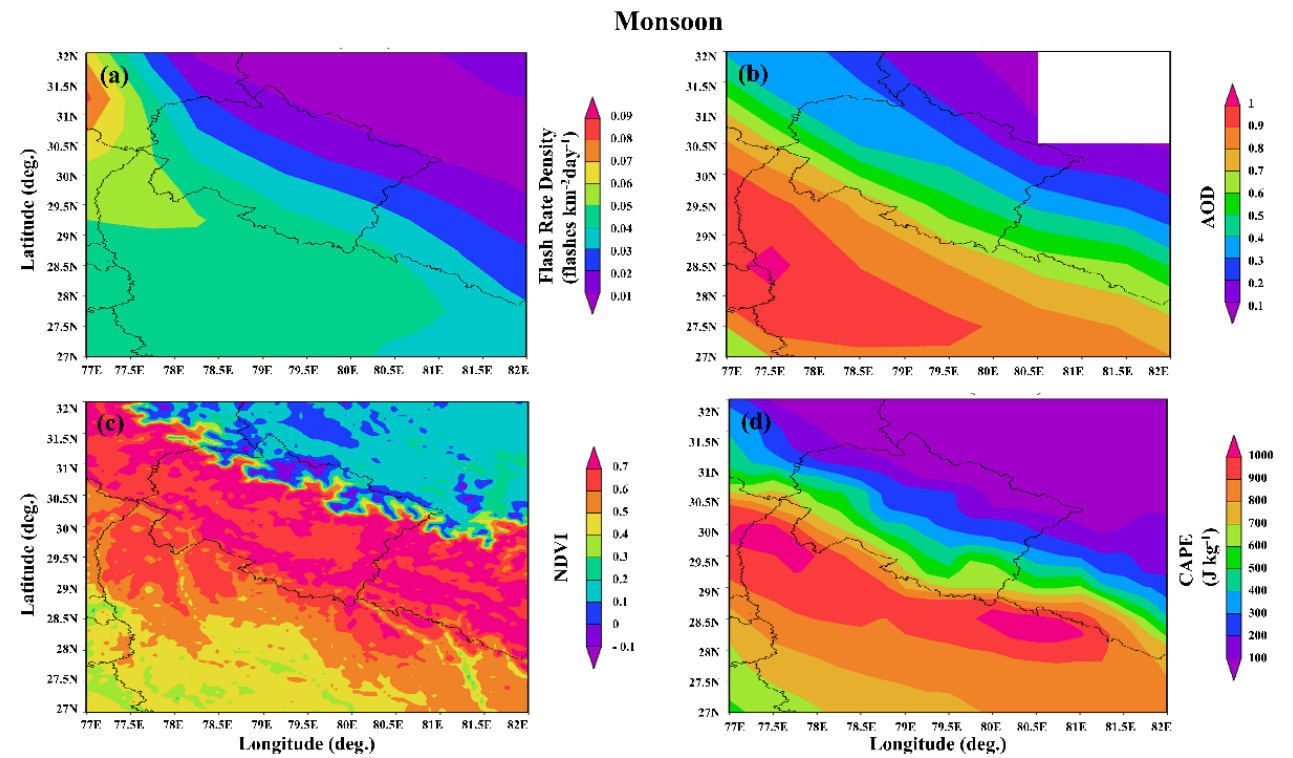


Figure 5. Spatial distribution of (a) LFRD, (b) AOD, (c) NDVI, and (d) CAPE for monsoon season over the study region.

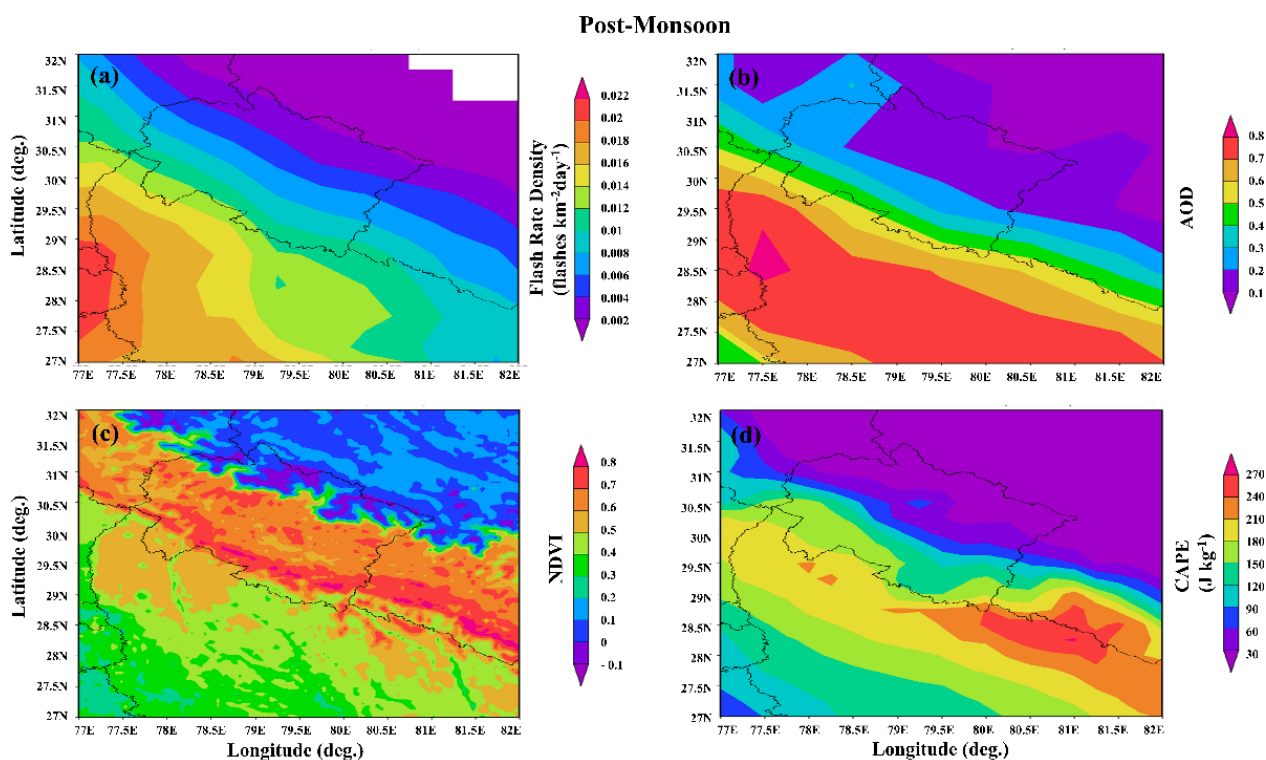


Figure 6. Spatial distribution of (a) LFRD, (b) AOD, (c) NDVI, and (d) CAPE for the post-monsoon season over the study region.

4.2. Dependency of Lightning on Thermodynamic Parameters

The dependency of the lightning flash rate on thermodynamical parameters, including surface air temperature, relative humidity, precipitation rate, vertical velocity, CAPE, NDVI, and AOD, has been determined using the Pearson correlation coefficient (Table 1). All the parameters showed a good positive correlation with the lightning flash rate, excluding precipitation and relative humidity, in the pre-monsoon season, with a significance level of 95%. The corresponding p values for a significance level of 95% ($p = 0.05$) are calculated along with the correlation coefficient. p -values less than 0.05 represent a significant correlation. A negative correlation (-0.65) was observed between lightning and NDVI during this season, which indicates reduced vegetation cover during the pre-monsoon season. More agricultural waste burning in plain regions of IGP and forest fire activities over the hilly regions of the central Himalayas observed, which leads to a reduction in vegetation cover and increased aerosol loading. A lower value of vegetation cover was reported over the dry NW region of Indian subcontinents [42]. A dry surface leads to the possibility of increased lightning activity in the future [55]. Another study also verified the higher lightning activities over dryer NW regions as compared to that over moist NE regions [26].

CAPE showed a good correlation with the lightning flash rate for winter, pre-monsoon, and post-monsoon seasons (0.73, 0.73, and 0.70, respectively), with a significant level of 95%. In the monsoon season significantly high value of CAPE is obtained, but there is a scarcity of lightning, which results in a low correlation (~ 0.03). During monsoon season, the scavenging process by precipitation causes a low aerosol concentration [59]; therefore, it has a low correlation with lightning.

Figure 7 shows the monthly climatological average of different parameters with the lightning flash rate density. Peak values of lightning flashes were obtained in May and June, while the CAPE values hit their maximum in August. CAPE tends to increase from April and follow the trend of lightning till June; after that, the lightning flash rate decreases continuously, but CAPE increases till September and drops significantly in October, with a minimum in December and January. Similarly, vertical updraft shows an increasing trend

till July; after that, it decreases in the following months. Higher humidity and precipitation rates are observed to be at their maximum during the monsoon season, which also showed an increased vegetation index.

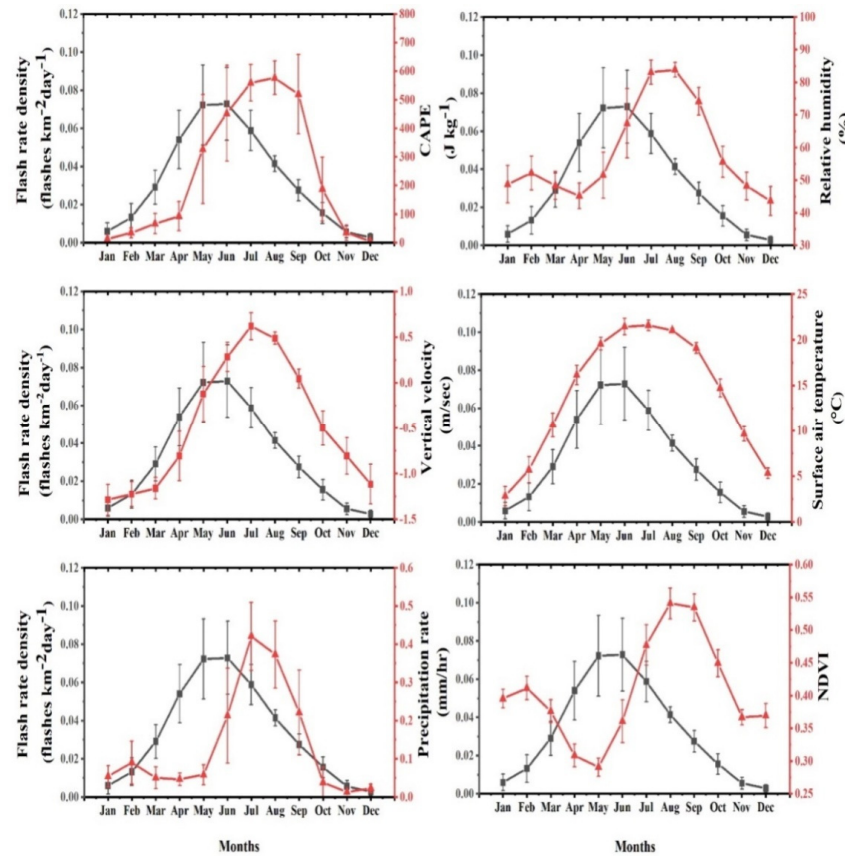


Figure 7. Monthly climatology for averaged values of flash rate density (on the primary Y-axis) with other parameters (on the secondary Y-axis) for the period of 2000–2013 over the study region.

Table 1. Pearson correlation coefficients between lightning flash rate density and other parameters for the period of 2000–2013 over the study region for winter, pre-monsoon, monsoon, and post-monsoon.

Parameters		Winter (DJF)	Pre-Monsoon (MAM)	Monsoon (JJAS)	Post-Monsoon (ON)
CAPE	cc (r)	0.73	0.74	0.03	0.70
	R ² (p-value)	0.54 (3.23 × 10 ⁻⁸)	0.54 (2.54 × 10 ⁻⁸)	0.0007 (0.84)	0.49 (3.37 × 10 ⁻⁵)
AOD	cc (r)	0.05	0.58	0.64	0.31
	R ² (p-value)	0.003 (0.74)	0.33 (6.53 × 10 ⁻⁵)	0.41 (1.15 × 10 ⁻⁷)	0.09 (0.12)
Precipitation Rate	cc (r)	0.75	0.41	0.03	0.46
	R ² (p-value)	0.56 (1.52 × 10 ⁻⁸)	0.16 (0.008)	0.0007 (0.85)	0.21 (0.01)
NDVI	cc (r)	0.58	-0.65	-0.73	0.73
	R ² (p-value)	0.34 (6.25 × 10 ⁻⁵)	0.42 (3 × 10 ⁻⁶)	0.53 (2.1 × 10 ⁻¹⁰)	0.53 (1.2 × 10 ⁻⁵)
Vertical velocity	cc (r)	0.05	0.76	0.32	0.41
	R ² (p-value)	0.003 (0.74)	0.57 (7.85 × 10 ⁻⁹)	0.11 (0.01)	0.17 (0.03)
Temperature	cc (r)	0.15	0.71	0.52	0.66
	R ² (p-value)	0.024 (0.33)	0.50 (1.86 × 10 ⁻⁷)	0.27 (3.63 × 10 ⁻⁵)	0.44 (1.2 × 10 ⁻⁴)
Relative Humidity	cc (r)	0.55	0.42	-0.13	0.70
	R ² (p-value)	0.30 (1.8 × 10 ⁻⁴)	0.17 (0.006)	0.02 (0.35)	0.48 (3.81 × 10 ⁻⁵)

4.3. Lightning and Aerosols

Figure 8 shows the time series of monthly average lightning flash rates with AOD over the study region. Two prominent peaks are observed in May 2001 and June 2011 for lightning flash rates, whereas the peaks of AOD are observed in July 2002 and July 2011. The fit straight lines in Figure 8 show a decreasing trend in LFRD and an increasing trend in aerosol loading. However, Figure 9 shows a positive correlation ($r = 0.58$, $p = 1.59 \times 10^{-16}$) between LFRD and AOD, with a significance level of 95%. In this figure, the yearly averaged time series of LFRD and AOD are plotted. Except for the early years of the study period, the average aerosol concentration over the study region follows the same trend as LFRD. There are matched peaks for the years 2008 and 2011, with subsequent drops in 2005, 2009, and 2012. A similar trend was reported over the IGP region [37]. A strong positive correlation with a variance of 58% has been found between LFRD and AOD. This is seen in the scatter plot between LFRD and AOD (Figure 10a). From this plot, it is also found that the critical value of AOD (0.2) represents the minimum value of AOD, which may act as aerosol charge particles responsible for the lightning activity over this region. From Figure 10a, it is also found that the value of AOD (0.3–0.5) is the most suitable range of aerosol charge particles for lightning over this region. The time series of flash per AOD (Figure 10b) also depicts that the maximum flash rate per AOD is observed in April and May, whereas the minimum is observed during the winter months (December, January, and February) of the year. In a recent study, Yadava et al. [60] analyzed 16 years (1998–2013) of lightning data and reported the maximum lightning events in the pre-monsoon season over northwestern parts of India. This ratio between LFRD and AOD indicates the amount of AOD responsible for lightning initiation.

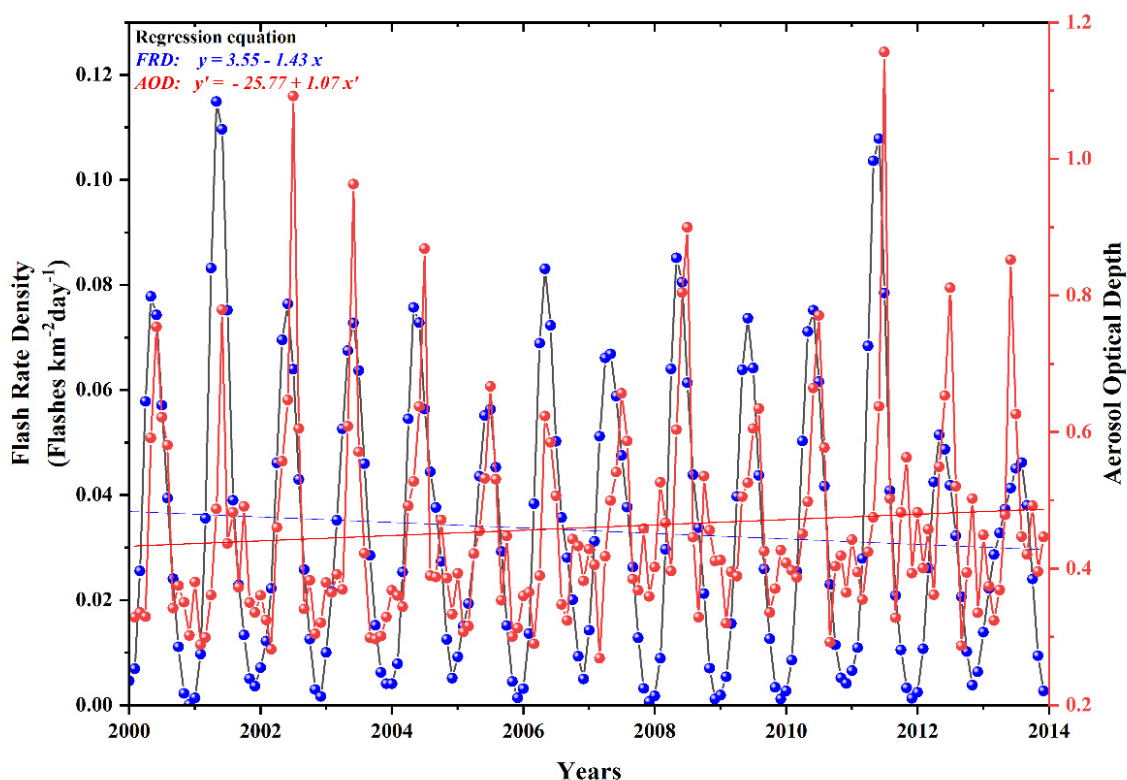


Figure 8. Monthly time series of lightning flash rate density (LFRD) and AOD from the year 2000 to 2013 over the study region.

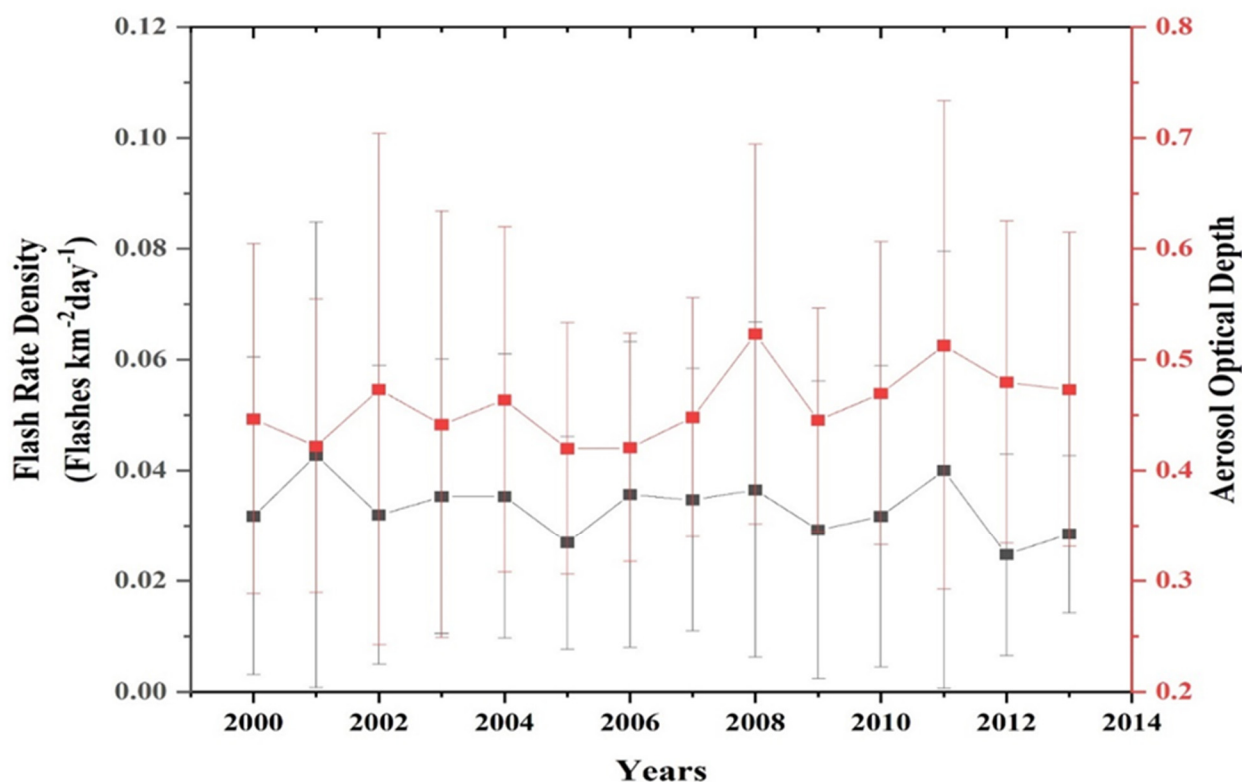


Figure 9. Annual variation for averaged values of lightning flash rate density (LFRD) (on the primary Y-axis) with AOD (on the secondary Y-axis) for the period of 2000–2013 over the study region.

The monthly climatology of LFRD with AOD is represented in Figure 11 and shows that the aerosol concentration tends to increase from March and reaches its maximum in July. The monsoon reaches the central Himalayan region in mid-June; after that, the aerosol concentration decreases significantly due to precipitation caused by the scavenging processes. The LFRD follows the increasing trend of aerosol during the pre-monsoon season, but it decreases during the monsoon period due to precipitation, which reduces the convective and lightning activity after July. The increased aerosol loading during pre-monsoon was found to be a combined effect of agricultural waste burning activity, forest fire, anthropogenic emission, and long-range transport, as well as containing desert soil/dust, organic matter, gaseous product (sulfate and nitrate), and soot particles [61]. A previous study has reported a similar pattern of increased lightning flash density over the land area of the Indian subcontinent during pre-monsoon months, with a peak in June, and the study also reported an increase in aerosol in July through external inflow and a sudden decrease in the subsequent months, possibly due to the monsoon precipitation [62].

Aerosol types are classified into different groups based on the correlation value of the aerosol optical depth (at 550 nm) and Ångström exponent (α) (412–470 nm) (Figure 12). The threshold values to classify the aerosol type were used earlier [63] under different synoptic meteorological conditions. The variation in the range depends on the aerosol type and sources of emission. In the present case, slightly different threshold values than previous studies [64] are used that are similar to those used for the Dehradun region [65]. Desert dust (DD) is associated with an AOD > 0.6 and α < 1.0, while clean condition (CC) is assigned to AOD < 0.2 and α > 0.5 values. Biomass burning (BB) is detected for AOD > 0.8 and α > 1.0. The range 0.3–0.8 of AOD with α > 1.0 is associated with anthropogenic aerosols (AAs), while the values of AOD and α within the range 0.2–0.6 and 0.4–1.0, respectively, are classified as mixed aerosols (MAs). The discrimination of well-mixed aerosols is a bit difficult. According to the above classification, most of the aerosol was found to be associated with anthropogenic sources, while the aerosols observed in pre-monsoon lie within the range of mixed as well as anthropogenic aerosols. The effect of biomass burning

is observed in the monsoon season. As per the literature, we know that higher values of α indicate the presence of fine-mode particles, while lower values correspond to the coarse-mode aerosol particles in the atmosphere [66]. Hence, from the scatter plot, it is found that a higher concentration of coarse particles during the pre-monsoon is a combined effect of anthropogenic, long-range transported, and mixed sources of aerosols. During post-monsoon and winter seasons, all emissions are confined to the local anthropogenic sources, with long-range transport from other regions being the least impactful. The accumulation of fine-mode ($\alpha \sim 0.8$), coarse-mode ($\alpha = 0.4\text{--}0.5$), and fine-mode ($\alpha = 0.7\text{--}0.8$) aerosol particles during winter, pre-monsoon, and post-monsoon seasons were classified, respectively, over the IGP in an earlier study [66]. Another study also suggested that the classification of aerosol observed for Gandhi College, Balia (India), and Kanpur (India) as desert dust ($\alpha < 0.7$), mixed-type ($\alpha = 0.7\text{--}1$), and fine-mode ($\alpha > 1.0$) aerosols [66]. Previous studies suggested that many regions show higher lightning activity during polluted days of AOD ranges ($0.2 < \text{AOD} < 0.4$) than clear days globally [61,62]. Wang et al. [14] discussed the impact of the type of aerosol on lightning under moist and dry climatic conditions and reported that lower values of AOD lightning are caused by aerosol–cloud interaction. On the other hand, for higher values of AOD, aerosol’s radiative effect plays an important role in the initiation of lightning [14]. In the present study, an increased lightning flash density is observed for the months of pre-monsoon and post-monsoon seasons, with AOD values corresponding to the range of 0.2–0.4, and mostly, the aerosols present during this period belong to the anthropogenic emissions.

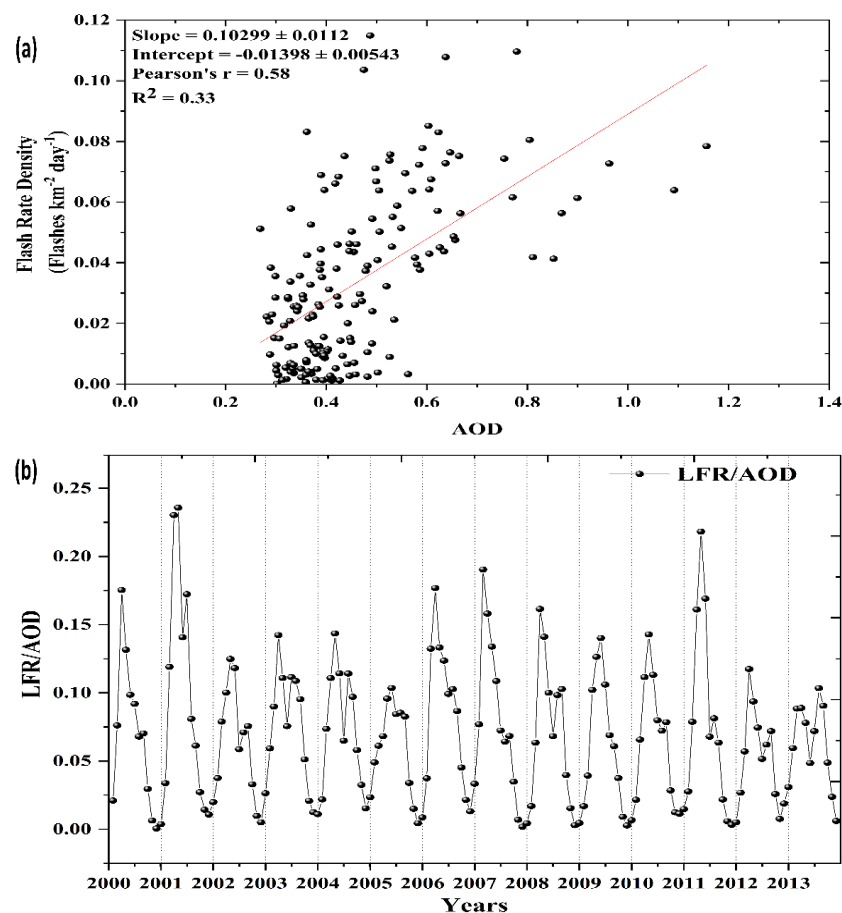


Figure 10. (a) Scatter plot between monthly flash rate density and AOD for the whole study period; (b) time series plot for the ratio of LFRD to the AOD of each month’s data from 2000 to 2013 over the study region.

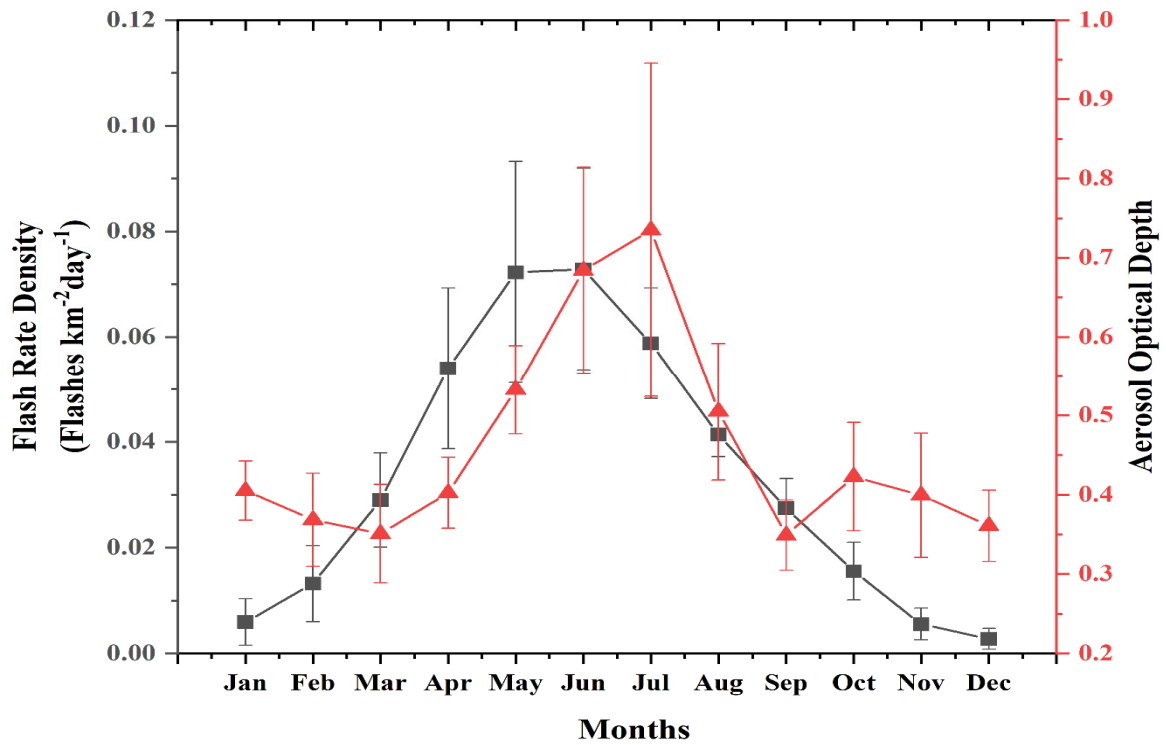


Figure 11. Monthly climatology for averaged values of the lightning flash rate density (on the primary Y-axis) with AOD (on the secondary Y-axis) for the period of 2000–2013 over the study region.

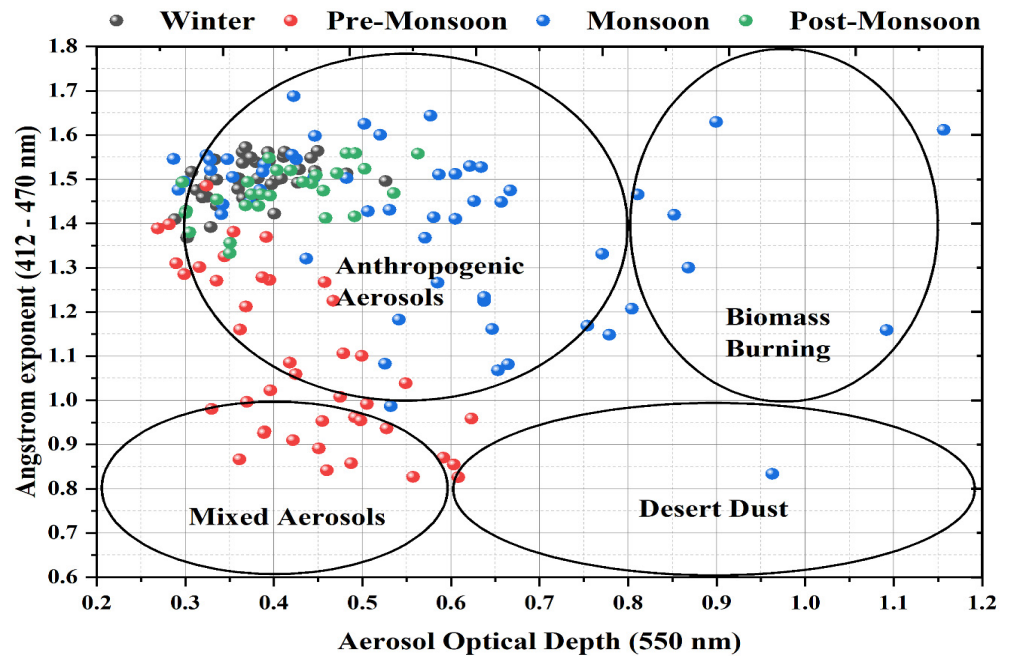


Figure 12. Scatter plot between the angstrom exponent (412–470 nm) and AOD (550 nm) for seasonally averaged values between the period 2000–2013 over the study region.

4.4. Spatial Variation of Proxy and the Future Projection of LFR

The dependency on the local thermodynamic phenomena is very high for the formation of lightning in any specific region. In the previous section, it was reported that the thermodynamic parameters such as CAPE, precipitation rate, temperature, and relative humidity are highly correlated with the lightning flash rate over the considered region. Therefore, for the determination of LFRD, we adopted a thermodynamic relation and used

it as a proxy. Figure 13 depicts the annual spatial distribution of the proxy and LFRD over the selected region. The spatial distribution of LFR is equivalent to the proxy, especially in the middle part of the study region. The spatial distribution of the proxy is highly matched over the northern part of Uttarakhand. The maximum amount of energy, i.e., $4 \text{ kg m}^{-2} \text{ day}^{-1}$, has been observed from the northern part of the region, which is spatially matched with the LFR distribution. This indicates that the maximum amount of energy is responsible for the formation of lightning. Chandra et al. [38] also describe the spatial distribution of LFRD and proxy for the Southeast Asian region.

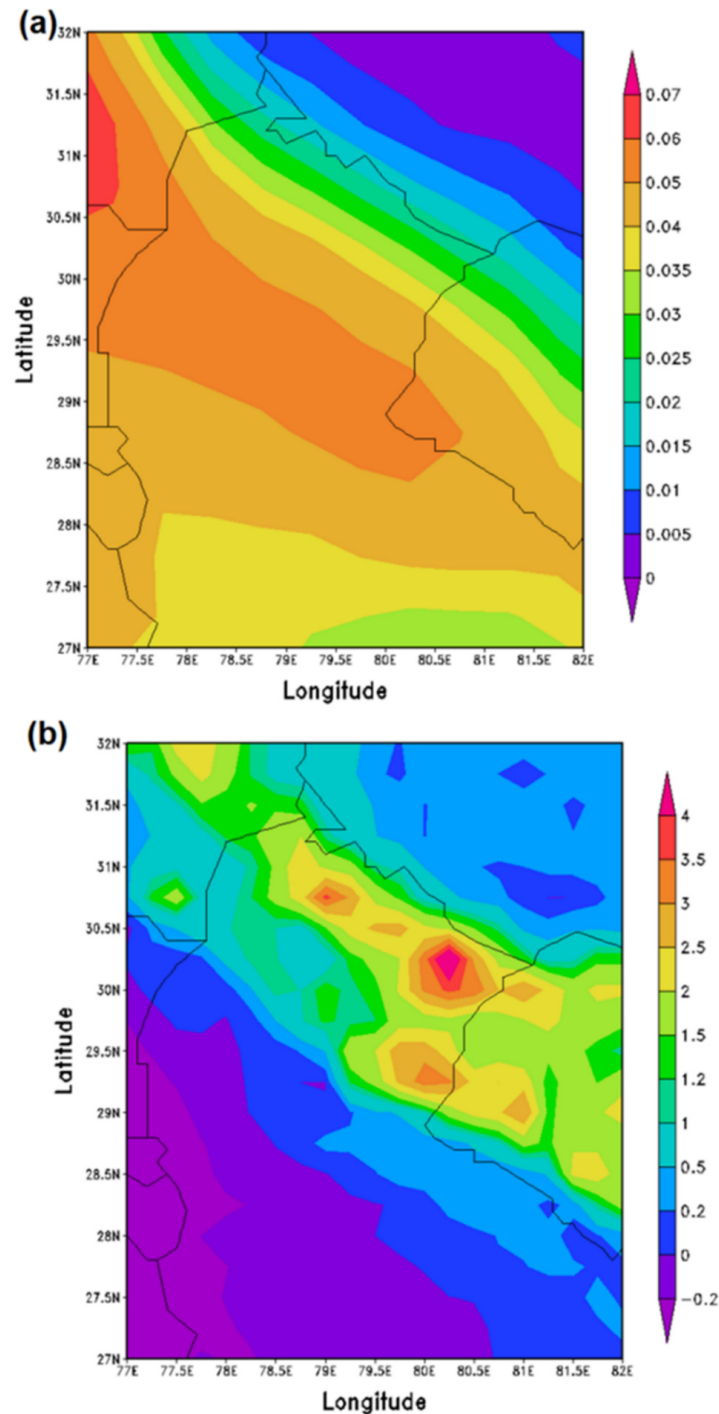


Figure 13. Spatial distribution of (a) LFR ($\text{flashes km}^{-2} \text{ day}^{-1}$); (b) proxy ($\text{kg m}^{-2} \text{ day}^{-1}$).

Using this proxy for projecting the LFR over the small part of the study region of Srinagar, it is observed that the maximum similarity is observed between the proxy and LFR, as seen from the spatial distribution in Figure 12. Because of large changes in the thermodynamic parameters and matching of the proxy to the LFRD, corresponding changes in lightning are expected in the future. Using the present data, the LFRD distribution for the late 21st century, from 2079 to 2088, is simulated and compared for this region as compared to the historic period (1996–2005). The difference in LFRD between the historic period and the annual simulated mean of the models at the end of the 21st century, assuming the Representative Concentrations Pathway-8.5 (RCP-8.5) scenario, has been taken for the determination of future increase/decrease in LFRD over the study region. Changes in the precipitation rate, evaporation rate, and atmospheric temperature are projected for the end of the 21st century from the historic period. However, the ensemble means of all the GCMs considered in this study are based on the assumptions that the precipitation, evaporation, and temperature will increase, with a mean increase of approximately 6.25%, 13.16%, and 2.3%, respectively, by the end of the 21st century over Srinagar, Uttarakhand. Using the method of percentage change between the years 1996–2005 and 2079–2088, the ensemble means of all GCMs predict that the annual mean LFRD is expected to increase in Srinagar, Uttarakhand, by 7.41%. Previously, many researchers estimated LFR in global warming scenarios over an extensive range and indicated both increasing/decreasing trends in lightning activity [19,24,35]. There is a well-known thermodynamic relation made by Romps et al. [67], using CAPE and the precipitation rate for the determination of LFRD over the CONUS region. In their experiment, they used CMIP5 model data in the RCP8.5 scenario to determine the future increase in cloud-to-ground lightning by 12% from 2079 to 2088 over the same region.

5. Summary and Conclusions

The occurrence of lightning over any specific region depends on local thermodynamic conditions, including local meteorological parameters, topography, and aerosols present in the atmosphere, in a complex manner. A significant difference was observed between the climatology and topography of the NW and NE regions of the Indian subcontinent. There is more lightning activity in the moist NE region at a lower terrain slope/elevation and with higher vegetation cover. The NE region has forest areas with deeper roots that hold more water and have higher latent heat fluxes. The highest leaf area in the forest permits more transpiration of water vapor into the air and, subsequently, produces higher CAPE and deeper convection. The large latent heat fluxes in the forested area have the potential to enhance convection. This may be one of the causes of enhanced lightning activity in the forest areas with the lower elevations in the moist environment of the NE region. As the study region is a part of the central Himalayas, the value of NDVI was observed in the intermediate range. Although the value of NDVI is observed to be low as compared to that in the moist region of NE and high in comparison to the NW dry region [42].

The dry NW region is more susceptible to lightning activity where terrain slope or elevation is more, even when there is little or no vegetation cover and low humidity. On the arrival of the monsoon in mid-June, over this region, humidity and convective activity tend to increase, but the lightning flashes seem to decrease during the monsoon season.

Aerosol concentration shows a good correlation with lightning flash rate density. It increases with more aerosol loading in the pre-monsoon season and decreases with the removal of aerosol during the monsoon. However, elevated AOD levels could not affect the lightning during the post-monsoon and winter seasons because of the possible lack of vertical updraft due to low temperatures and shallow boundary layer height. The indirect effect of aerosol loading on the atmosphere includes the change in the radiation budget of the atmosphere. The vertical motion of air regulates the water vapor content and change in moisture gradient, which may result in intense electrification in convective clouds. Lightning activity over this region seems to be a combined effect of aerosol loading, vertical motion of air, and surface temperature. Additionally, the thermodynamic parameters such

as precipitation, evaporation, and surface fluxes play an important role in the formation of convective activity over here. Therefore, the defined proxy is used for the projection of lightning over Srinagar as the first attempt. We found a positive result of the proxy over LFRD; therefore, we used it for the projection of LFRD in the late 21st century. Overall, using the RCP8.5 scenario, the GCMs predict a 7.41% increase in the LFRD in Srinagar, Uttarakhand, during the end of the 21st century.

Most of the lightning events occur in hilly regions, but due to the low population density over hilly regions, the number of lightning-related fatalities is also low. Plane areas with a high population density are more susceptible to higher fatality by a lightning strike [19]. According to a recent study, Uttar Pradesh (India) falls in the <5 range in the ranking of states with lightning-related fatalities, while Uttarakhand is between the 16–20 range. In the study region, the maximum lightning observed during the pre-monsoon period coincides with the crop cultivation season. Farmers and workers who have been working in the open fields are more prone to be affected by a lightning strike. High altitude places and mountain peaks result in much-reduced distance between surface and cloud, which leads to an easy target for lightning-induced damage.

In the future, the study of ground-based observation of lightning would be helpful in the mitigation of lightning-related fatality over the Uttarakhand (India) region of the central Himalayas, but presently no ground-based data on lightning is available for the study region. It will also improve the understanding of the causality of lightning-related events.

Author Contributions: A.S.G.: Conceptualization, Methodology, Formal analysis, Investigation, writing—review and revising the original draft, A.J.: Conceptualization, Methodology, Formal analysis, Investigation, Writing—original draft. S.C.: Conceptualization, Writing—review and editing. U.C.D.: Editing and revising. D.S.: Editing and revising. R.P.S.: Editing & revising. All authors have read and agreed to the published version of the manuscript.

Funding: The present study has no external funding.

Institutional Review Board Statement: Not applicable.

Informed Consent Statement: Not applicable.

Data Availability Statement: Data can be available after request. The MODIS observations were downloaded from the MODIS database (<https://giovanni.gsfc.nasa.gov/giovanni/> (accessed on 1 September 2021)). The lightning data TRMM LIS/OTD platform was downloaded from the website (https://ghrc.nsstc.nasa.gov/lightning/data/data_lis_trmm.html (accessed on 15 July 2021)). All the thermodynamical parameters were downloaded from the ECMWF ERA 5 platform (<https://www.ecmwf.int/en/forecasts/datasets/reanalysis-datasets/era5> (accessed on 1 September 2021)).

Acknowledgments: A.S.G. and A.J. would like to thank the Department of Science and Technology (DST), Government of India, for funding support under the Climate Change Programme (CCP), SPLICE Division (DST/CCP/Aerosol/83/2017(G)). We would like to thank the Vice-Chancellor of HNBGU Srinagar and the Head of the Department of Physics, HNBGU Srinagar, for providing the necessary infrastructure facility and guidance for this study. We are thankful to the editor, Estella Wang, and two anonymous reviewers for providing valuable suggestions and improving the scientific quality of the manuscript.

Conflicts of Interest: The authors declare no conflict of interest.

References

1. Michalon, N.; Nassif, A.; Saouri, T.; Royer, J.F.; Pontikis, C.A. Contribution to the climatological study of lightning. *Geophys. Res. Lett.* **1999**, *26*, 3097–3100. [[CrossRef](#)]
2. Boccippio, D.J.; Goodman, S.J.; Heckman, S. Regional differences in tropical lightning distributions. *J. Appl. Meteorol.* **2000**, *39*, 2231–2248. [[CrossRef](#)]
3. Orville, R.E.; Huffines, G.; Nielsen-Gammon, J.; Zhang, R.; Ely, B.; Steiger, S.; Phillips, S.; Allen, S.; Read, W. Enhancement of cloud-to-ground lightning over Houston, Texas. *Geophys. Res. Lett.* **2001**, *28*, 2597–2600. [[CrossRef](#)]
4. Williams, E.; Stanfill, S. The physical origin of the land-ocean contrast in lightning activity. *Comptes Rendus Phys.* **2002**, *3*, 1277–1292. [[CrossRef](#)]

5. Christian, H.J.; Blakeslee, R.J.; Boccippio, D.J.; Boeck, W.L.; Buechler, D.E.; Driscoll, K.T.; Goodman, S.J.; Hall, J.M.; Koshak, W.J.; Mach, D.M.; et al. Global frequency and distribution of lightning as observed from space by the Optical Transient Detector. *J. Geophys. Res. Atmos.* **2003**, *108*, ACL 4-1. [[CrossRef](#)]
6. Williams, E.; Mushtak, V.; Rosenfeld, D.; Goodman, S.; Boccippio, D. Thermodynamic conditions favorable to superlative thunderstorm updraft, mixed phase microphysics and lightning flash rate. *Atmos. Res.* **2005**, *76*, 288–306. [[CrossRef](#)]
7. Bell, T.L.; Rosenfeld, D.; Kim, K.M. Weekly cycle of lightning: Evidence of storm invigoration by pollution. *Geophys. Res. Lett.* **2009**, *36*. [[CrossRef](#)]
8. Bell, T.L.; Rosenfeld, D.; Kim, K.M.; Yoo, J.M.; Lee, M.I.; Hahnenberger, M. Midweek increase in U.S. summer rain and storm heights suggests air pollution invigorates rainstorms. *J. Geophys. Res. Atmos.* **2008**, *113*, 1–22. [[CrossRef](#)]
9. Guo, J.; Deng, M.; Lee, S.S.; Wang, F.; Li, Z.; Zhai, P.; Liu, H.; Lv, W.; Yao, W.; Li, X. Delaying precipitation and lightning by air pollution over the Pearl River Delta. Part I: Observational analyses. *J. Geophys. Res. Atmos.* **2016**, *121*, 6472–6488. [[CrossRef](#)]
10. Tao, W.K.; Chen, J.P.; Li, Z.; Wang, C.; Zhang, C. Impact of aerosols on convective clouds and precipitation. *Rev. Geophys.* **2012**, *50*, 1–62. [[CrossRef](#)]
11. Fan, J.; Wang, Y.; Rosenfeld, D.; Liu, X. Review of aerosol-cloud interactions: Mechanisms, significance, and challenges. *J. Atmos. Sci.* **2016**, *73*, 4221–4252. [[CrossRef](#)]
12. Li, Z.; Lau, W.K.M.; Ramanathan, V.; Wu, G.; Ding, Y.; Manoj, M.G.; Liu, J.; Qian, Y.; Li, J.; Zhou, T.; et al. Aerosol and monsoon climate interactions over Asia. *Rev. Geophys.* **2016**, *54*, 866–929. [[CrossRef](#)]
13. Li, Z.; Guo, J.; Ding, A.; Liao, H.; Liu, J.; Sun, Y.; Wang, T.; Xue, H.; Zhang, H.; Zhu, B. Aerosol and boundary-layer interactions and impact on air quality. *Natl. Sci. Rev.* **2017**, *4*, 810–833. [[CrossRef](#)]
14. Wang, Q.; Li, Z.; Guo, J.; Zhao, C.; Cribb, M. The climate impact of aerosols on the lightning flash rate: Is it detectable from long-term measurements? *Atmos. Chem. Phys.* **2018**, *18*, 12797–12816. [[CrossRef](#)]
15. Zhao, P.; Zhou, Y.; Xiao, H.; Liu, J.; Gao, J.; Ge, F. Total lightning flash activity response to aerosol over China area. *Atmosphere* **2017**, *8*, 26. [[CrossRef](#)]
16. Zhang, R.; Li, G.; Fan, J.; Wu, D.L.; Molina, M.J. Intensification of Pacific storm track linked to Asian pollution. *Proc. Natl. Acad. Sci. USA* **2007**, *104*, 5295–5299. [[CrossRef](#)]
17. Siingh, D.; Singh, R.P.; Kumar, S.; Dharmaraj, T.; Singh, A.K.; Singh, A.K.; Patil, M.N.; Singh, S. Lightning and middle atmospheric discharges in the atmosphere. *J. Atmos. Sol. Terr. Phys.* **2015**, *134*, 78–101. [[CrossRef](#)]
18. Williams, E.R. Lightning and climate: A review. *Atmos. Res.* **2005**, *76*, 272–287. [[CrossRef](#)]
19. Finney, D.L.; Doherty, R.M.; Wild, O.; Stevenson, D.S.; MacKenzie, I.A.; Blyth, A.M. A projected decrease in lightning under climate change. *Nat. Clim. Chang.* **2018**, *8*, 210–213. [[CrossRef](#)]
20. Rosenfeld, D. TRMM observed first direct evidence of smoke from forest fires inhibiting rainfall. *Geophys. Res. Lett.* **1999**, *26*, 3105–3108. [[CrossRef](#)]
21. Andreae, M.O.; Rosenfeld, D.; Artaxo, P.; Costa, A.A.; Frank, G.P.; Longo, K.M.; Silva-Dias, M.A.F. Smoking Rain Clouds over the Amazon. *Science* **2004**, *303*, 1337–1342. [[CrossRef](#)]
22. Koren, I.; Kaufman, Y.J.; Rosenfeld, D.; Remer, L.A.; Rudich, Y. Aerosol invigoration and restructuring of Atlantic convective clouds. *Geophys. Res. Lett.* **2005**, *32*, 1–4. [[CrossRef](#)]
23. Siingh, D.; Singh, A.K.; Patel, R.P.; Singh, R.; Singh, R.P.; Veenadhari, B.; Mukherjee, M.; Siingh, D.; Singh, A.K.; Patel, R.P.; et al. Thunderstorms, Lightning, Sprites and Magnetospheric Whistler-Mode Radio Waves. *SGeo* **2008**, *29*, 499–551. [[CrossRef](#)]
24. Siingh, D.; Kumar, P.R.; Kulkarni, M.N.; Singh, R.P.; Singh, A.K. Lightning, convective rain and solar activity—Over the South/Southeast Asia. *Atmos. Res.* **2013**, *120–121*, 99–111. [[CrossRef](#)]
25. Sekiguchi, M.; Hayakawa, M.; Nickolaenko, A.P.; Hobara, Y. Evidence on a Link between the Intensity of Schumann Resonance and Global Surface Temperature. *Copernic. GmbH: Göttingen.* **2006**, *24*, 1809–1817. [[CrossRef](#)]
26. Kumar, P.R.; Kamra, A.K. The spatiotemporal variability of lightning activity in the Himalayan foothills. *J. Geophys. Res. Atmos.* **2012**, *117*, 24201. [[CrossRef](#)]
27. Ramesh Kumar, P.; Kamra, A.K. Land-sea contrast in lightning activity over the sea and peninsular regions of South/Southeast Asia. *Atmos. Res.* **2012**, *118*, 52–67. [[CrossRef](#)]
28. Penki, R.K.; Kamra, A.K. The lightning activity associated with the dry and moist convections in the Himalayan Regions. *J. Geophys. Res. Atmos.* **2013**, *118*, 6246–6258. [[CrossRef](#)]
29. Yuan, T.; Qie, X. Study on lightning activity and precipitation characteristics before and after the onset of the South China Sea summer monsoon. *J. Geophys. Res. Atmos.* **2008**, *113*, 14101. [[CrossRef](#)]
30. Dey, S.; Girolamo, L. Di A climatology of aerosol optical and microphysical properties over the Indian subcontinent from 9 years (2000–2008) of Multiangle Imaging Spectroradiometer (MISR) data. *J. Geophys. Res. Atmos.* **2010**, *115*, 15204. [[CrossRef](#)]
31. Kilinc, M.; Beringer, J. The spatial and temporal distribution of lightning strikes and their relationship with vegetation type, elevation, and fire scars in the northern Territory. *J. Clim.* **2007**, *20*, 1161–1173. [[CrossRef](#)]
32. Emanuel, K.A. *Atmospheric Convection*; Oxford University Press on Demand: Oxford, UK, 1994.
33. Handbook of Atmospheric Electrodynamics. Available online: <https://www.taylorfrancis.com/books/edit/10.1201/9780203719503/handbook-atmospheric-electrodynamics-hans-volland> (accessed on 3 March 2022).
34. Williams, E.; Renno, N. An Analysis of the Conditional Instability of the Tropical Atmosphere. *Mon. Weather Rev.* **1993**, *121*, 21–36. [[CrossRef](#)]

35. Clark, S.K.; Ward, D.S.; Mahowald, N.M. Parameterization-based uncertainty in future lightning flash density. *Geophys. Res. Lett.* **2017**, *44*, 2893–2901. [CrossRef]
36. Siingh, D.; Buchunde, P.S.; Singh, R.P.; Nath, A.; Kumar, S.; Ghodpage, R.N. Lightning and convective rain study in different parts of India. *Atmos. Res.* **2014**, *137*, 35–48. [CrossRef]
37. Lal, D.M.; Ghude, S.D.; Mahakur, M.; Waghmare, R.T.; Tiwari, S.; Srivastava, M.K.; Meena, G.S.; Chate, D.M. Relationship between aerosol and lightning over Indo-Gangetic Plain (IGP), India. *Clim. Dyn.* **2018**, *50*, 3865–3884. [CrossRef]
38. Chandra, S.; Siingh, D.; Jeni Victor, N.; Kamra, A.K. Lightning activity over South/Southeast Asia: Modulation by thermodynamics of lower atmosphere. *Atmos. Res.* **2021**, *250*, 105378. [CrossRef]
39. Qie, X.; Toumi, R.; Yuan, T. Lightning activities on the Tibetan Plateau as observed by the lightning imaging sensor. *J. Geophys. Res. Atmos.* **2003**, *108*. [CrossRef]
40. Price, C. Global Thunderstorm activity. In *Sprites, Elves and Intense Lightning Discharges*; Kluwer Academic Publishers: Amsterdam, The Netherlands, 2006; pp. 85–99.
41. Guo, J.; Yan, Y.; Chen, D.; Lv, Y.; Han, Y.; Guo, X.; Liu, L.; Miao, Y.; Chen, T.; Nie, J.; et al. The response of warm-season precipitation extremes in China to global warming: An observational perspective from radiosonde measurements. *Clim. Dyn.* **2020**, *54*, 3977–3989. [CrossRef]
42. Oulkar, S.; Siingh, D.; Saha, U.; Kamra, A.K. Distribution of lightning in relation to topography and vegetation cover over the dry and moist regions in the Himalayas. *J. Earth Syst. Sci.* **2019**, *128*, 180. [CrossRef]
43. Medina, S.; Houze, R.A.; Kumar, A.; Niyogi, D. Summer monsoon convection in the Himalayan region: Terrain and land cover effects. *Q. J. R. Meteorol. Soc.* **2010**, *136*, 593–616. [CrossRef]
44. Albrecht, R.I.; Goodman, S.J.; Buechler, D.E.; Blakeslee, R.J.; Christian, H.J. Where are the lightning hotspots on earth? *Bull. Am. Meteorol. Soc.* **2016**, *97*, 2051–2068. [CrossRef]
45. Chaudhari, H.S.; Ranalkar, M.; Chaudhari, H.S.; Ranalkar, M.R.; Kumkar, Y.V.; Oh, J.H.; Singh, G.P. Study of Lightning Activity Over Indian Subcontinent. In *Advances in Geosciences*; World Scientific: Singapore, 2008; Volume 16. Available online: https://www.worldscientific.com/doi/10.1142/9789812838100_0011 (accessed on 24 August 2022).
46. Cecil, D.J.; Buechler, D.E.; Blakeslee, R.J. Gridded lightning climatology from TRMM-LIS and OTD: Dataset description. *Atmos. Res.* **2014**, *135–136*, 404–414. [CrossRef]
47. Acker, J.G.; Leptoukh, G. Online analysis enhances use of NASA Earth Science Data. *Eos* **2007**, *88*, 14–17. [CrossRef]
48. Hersbach, H.; Bell, B.; Berrisford, P.; Hirahara, S.; Horányi, A.; Muñoz-Sabater, J.; Nicolas, J.; Peubey, C.; Radu, R.; Schepers, D.; et al. The ERA5 global reanalysis. *Q. J. R. Meteorol. Soc.* **2020**, *146*, 1999–2049. [CrossRef]
49. Roy, I.; Tedeschi, R.G. Influence of ENSO on regional Indian summer monsoon precipitation-local atmospheric influences or remote influence from Pacific. *Atmosphere* **2016**, *7*, 25. [CrossRef]
50. Roy, I.; Tedeschi, R.G.; Collins, M. ENSO teleconnections to the Indian summer monsoon in observations and models. *Int. J. Climatol.* **2017**, *1813*, 1794–1813. [CrossRef]
51. Roy, I.; Gagnon, A.S.; Siingh, D. Evaluating ENSO teleconnections using observations and CMIP5 models. *Theor. Appl. Climatol.* **2019**, *136*, 1085–1098. [CrossRef]
52. Roy, I. Indian Summer Monsoon and El Niño Southern Oscillation in CMIP5 models: A few areas of agreement and disagreement. *Atmosphere* **2017**, *8*, 154. [CrossRef]
53. Bonan, G.B. Forests and climate change: Forcings, feedbacks, and the climate benefits of forests. *Science* **2008**, *320*, 1444–1449. [CrossRef]
54. Kumar, S.; Siingh, D.; Singh, R.P.; Singh, A.K. The influence of meteorological parameters and atmospheric pollutants on lightning, rainfall, and normalized difference vegetation index in the Indo-Gangetic Plain. *Int. J. Remote Sens.* **2016**, *37*, 53–77. [CrossRef]
55. Pielke, R.A. Influence of the spatial distribution of vegetation and soils on the prediction of cumulus Convective rainfall. *Rev. Geophys.* **2001**, *39*, 151–177. [CrossRef]
56. Kar, J.; Deeter, M.N.; Fishman, J.; Liu, Z.; Omar, A.; Creilson, J.K.; Trepte, C.R.; Vaughan, M.A.; Winker, D.M. Wintertime pollution over the Eastern Indo-Gangetic Plains as observed from MOPITT, CALIPSO and tropospheric ozone residual data. *Atmos. Chem. Phys.* **2010**, *10*, 12273–12283. [CrossRef]
57. Di Girolamo, L.; Bond, T.C.; Bramer, D.; Diner, D.J.; Fettingner, F.; Kahn, R.A.; Martonchik, J.V.; Ramana, M.V.; Ramanathan, V.; Rasch, P.J. Analysis of multi-angle Imaging SpectroRadiometer (MISR) aerosol optical depths over greater India during winter 2001–2004. *Geophys. Res. Lett.* **2004**, *31*, 1–5. [CrossRef]
58. Jethva, H.; Satheesh, S.K.; Srinivasan, J. Seasonal variability of aerosols over the Indo-Gangetic basin. *J. Geophys. Res. Atmos.* **2005**, *110*, 1–15. [CrossRef]
59. Singh, D.K.; Singh, R.P.; Kamra, A.K. The electrical environment of the Earth’s atmosphere: A review. *Space Sci. Rev.* **2004**, *113*, 375–408. [CrossRef]
60. Yadava, P.K.; Soni, M.; Verma, S.; Kumaret, H.; Sharma, A.; Payra, S. The major lightning regions and associated casualties over India. *Nat. Hazards.* **2020**, *101*, 217–229. [CrossRef]
61. Srivastava, A.K.; Ram, K.; Pant, P.; Hegde, P.; Joshi, H. Black carbon aerosols over Manora Peak in the Indian Himalayan foothills: Implications for climate forcing. *Environ. Res. Lett.* **2012**, *7*, 014002. [CrossRef]
62. Pal, J.; Chaudhuri, S.; Chowdhury, A.R.; Bandyopadhyay, T. Cloud—Aerosol interaction during lightning activity over land and ocean: Precipitation pattern assessment. *Asia-Pac. J. Atmos. Sci.* **2016**, *52*, 251–261. [CrossRef]

63. Kaskaoutis, D.G.; Kambezidis, H.D.; Hatzianastassiou, N.; Kosmopoulos, P.G.; Badarinath, K.V.S. Aerosol climatology: On the discrimination of aerosol types over four AERONET sites. *Atmos. Chem. Phys. Discuss.* **2007**, *7*, 6357–6411.
64. Kaskaoutis, D.G.; Badarinath, K.V.S.; Kharol, S.K.; Sharma, A.R.; Kambezidis, H.D. Variations in the aerosol optical properties and types over the tropical urban site of Hyderabad, India. *J. Geophys. Res. Atmos.* **2009**, *114*, 22204. [[CrossRef](#)]
65. Patel, P.N.; Kumar, R. Estimation of Aerosol Characteristics and Radiative Forcing during Dust Events over Dehradun. *Aerosol Air Qual. Res.* **2015**, *15*, 2082–2093. [[CrossRef](#)]
66. Kedia, S.; Ramachandran, S.; Holben, B.N.; Tripathi, S.N. Quantification of aerosol type, and sources of aerosols over the Indo-Gangetic Plain. *Atmos. Environ.* **2014**, *98*, 607–619. [[CrossRef](#)]
67. Romps, D.M.; Seeley, J.T.; Vollaro, D.; Molinari, J. Projected increase in lightning strikes in the united states due to global warming. *Science* **2014**, *346*, 851–854. [[CrossRef](#)] [[PubMed](#)]